Localized Corrosion Suppression in Stationary-Shoulder Friction-Stir-Processed AZ31B Magnesium Alloy

William W. Predebon[1] and Sanjana Sharma[2,*]

[1] Retired professor and chair of the Department of Mechanical Engineering-Engineering Mechanics, at Michigan Technological University
[2] Department of Mechanical Engineering-Engineering Mechanics, at Michigan Technological University
* Correspondence: sanjsharma@gmail.com

Abstract: Stationary shoulder friction stir processing (SSFSP) is a new surface modification method for magnesium alloys with minimal heat input. However, the corrosion advantage of SSFSP should be evaluated in terms of the electrochemical rate and corrosion morphology. The key issue is to determine if SSFSP prevents localized corrosion in the AZ31B magnesium alloy under chloride environment by creating a homogeneous stirring layer through the entire thickness. Commercial plates of AZ31B of 6.35 mm thick were processed by SSFSP technique with H13 steel tool under stationary shoulder and rotating probe with the speed of 700 rpm and travel of 100 mm/min. The corrosion resistance of base material and the surface of stir layer in the deaerated 3.5 wt% NaCl solution was tested by OCP measurement, potentiodynamic polarization, and SEM/EDS analysis after corrosion. In this paper, experimental results show that the mean grain size in the base material reduced from 25.2 ± 2.2 µm to 6.34 ± 0.12 µm (74.84% reduction with grain-size inversion factor of 3.97). The corrosion current density decreased from 9.815×10^{-3} to 2.032×10^{-3} A/cm^2, and the corrosion potential kept stable value around -0.546 V. On the other hand, OCP of processed area formed a steady-state band of -0.40 V ~ -0.35 V, whereas base metal showed much wider fluctuations between -0.65 and -0.47 V. Morphology is able to answer the primary question regarding SSFSP – it is not simply about slowing down the average electrochemical reaction rate but rather changing the governing corrosion mechanism from a pitting one characterized by enhanced localized action to a corrosion product film mechanism with mud cracking and no pits at all. Hence, the enhancement of corrosion resistance results from the synergy of grain refinement, reduction in microgalvanic continuity, fragmentation of Al-Mn-Fe clusters, and absence of thermal asymmetry through the material thickness.

Keywords: AZ31B magnesium alloy; stationary-shoulder friction stir processing; chloride corrosion; grain refinement; localized corrosion; open-circuit potential; potentiodynamic polarization; corrosion morphology

Citation: William W. Predebon and Sanjana Sharma. 2022. Localized Corrosion Suppression in Stationary-Shoulder Friction-Stir-Processed AZ31B Magnesium Alloy. *TK Techforum Journal (ThyssenKrupp Techforum)* 2022(2): 18–41.

Received: February-18-2022
Accepted: July-29-2022
Published: September-30-2022

1. Introduction

Magnesium alloys hold a special place in lightweight engineering due to their relatively low density, which allows considerable weight savings in the automotive industry, consumer electronics, aerospace, and medical applications. However, the very same electrochemical reactivity of magnesium makes its application difficult in the presence of chlorides, since magnesium alloys in such solutions may form metastable corrosion products, cause alkalization, evolve hydrogen, and exhibit strong micro-galvanic effects between the alpha phase of magnesium and the cathodic intermetallics. As a result, the alloy becomes prone to pitting or intergranular corrosion even if the overall dissolution rate is modest [1–4].

Therefore, in addition to chemical considerations, the issue of corrosion resistance of magnesium alloys requires careful examination of processing conditions and how they affect the microstructure and, thus, the electrochemical properties of the material. Previous studies in the field showed that the role of cathodic intermetallic phases in forming microgalvanic cells, the destabilizing effect of chloride ions on magnesium hydroxide protective

layers, and the role of path lengths between anodic and cathodic sites in controlling localized corrosion were already known. While grain refinement may positively influence magnesium corrosion by making the microstructure more homogeneous and interrupting corrosion paths, it was demonstrated that the effect of processing on the corrosion resistance may be negative if the process results in bimodal grain size distribution, residual tensile stresses, large texture gradients, and/or clustering of cathodic particles [5–7]. Therefore, evaluation of corrosion resistance due to processing should take into account not just the current density but also the mechanisms of corrosion propagation in processed materials.

Since friction stir processing (FSP) operates in the solid state, it provides excellent control of surface microstructure by means of severe plastic deformations, frictional heating, and dynamic recrystallization. In recent years, reviews of FSP revealed that the main areas of its application are grain refinement, surface composite fabrication, superplasticity, cast structure modification, and mechanical property enhancement [8–10]. In the case of magnesium alloys, FSP may break down particles, redistribute solutes, modify basal texture, and refine grains to equiaxed morphology. Since magnesium alloys are very sensitive to local galvanic coupling between the alpha phase and particles, connectivity of boundaries, and stability of corrosion product layers, these changes have obvious implications for magnesium corrosion [11–15].

The processing window of magnesium is narrow in FSP. In conventional rotating-shoulder FSP, heating is done via the shoulder as well as via the probe. It is necessary for plasticization, but excessive surface heat input, arc corrugation, flash formation, through-thickness asymmetry or even grain coarsening can occur due to an uncontrolled thermal cycle. Surface cooling during FSP has been explored in several studies of magnesium alloys to mitigate grain growth and maintain fine-grained structure, but the addition of cooling adds complexity to the process and may not necessarily guarantee uniform depth-dependent property enhancement [16,17]. Hence, a tool design concept that can reduce heat input at the surface while maintaining probe-induced deformation is preferable for thick sections and heat sensitive materials.

In this regard, stationary-shoulder friction stir processing offers an interesting possibility for thick plates and difficult-to-process materials. Stationary shoulder FSP utilizes a non-rotating shoulder in conjunction with a rotating probe. The shoulder holds and wipes the surface of the metal while the probe does the major part of the stirring and deformation process. The separation of functions results in reduced surface frictional heating and minimized through-thickness temperature gradient. Earlier studies have shown smooth surface and lower heat input from the shoulder, resulting in enhanced uniformity of grain refinement when compared with a rotating shoulder in conventional FSP [18–20]. The question to answer in this study is whether the observed benefits of stationary shoulder FSP lead to improved corrosion resistance.

A simple means to explore this question would be to expose magnesium alloy processed with stationary shoulder FSP to corrosive environment. To this end, samples made of AZ31B magnesium alloy subjected to stationary shoulder FSP were immersed in 3.5 wt% NaCl solution. The experimental evidence includes the surface morphology of the sample, microstructure and grain size variation across the section of the sample, open circuit potential, polarization curves and post-corrosion SEM/EDS analysis [21]. It can then be asked whether a stationary shoulder leads to a spatial corrosion mode switch in AZ31B, shifting from pits dominating the attack to a more uniform surface film behavior. This is crucial since most of the time the occurrence of the first penetrating defect becomes the limiting factor for service failure in magnesium components rather than the average weight loss per unit surface area.

To rigorously demonstrate the conclusion, three layers of evidence have to come together. On the first level, this is the processing data: the stationary shoulder, rotating threaded probe, 700 rpm rotation, 100 mm/min traverse, and 6.35 mm thickness of the specimen form the thermal-mechanical conditions for producing the stir zone. On the second level, this is the grain refinement, as evidenced by the significant reduction from

25.2 ± 2.2 to 6.34 ± 0.12 µm. On the third level, this is the corrosion morphology, as the identical corrosion potentials may well correspond to vastly different forms of damage. Base metal characterized by deep and numerous pits and SSFSP stir zone characterized by distributed corrosion product cannot be considered equal just because their corrosion potentials are similar.

In this analysis, corrosion parameters connect the experimental processing conditions with the resulting morphology. The measured values are used for calculating transparent improvement ratios which, in turn, have to be considered with regard to the pit distribution, the presence of mud cracks, the nature of intergranular damage, and the extent of corrosion products coverage. The underlying mechanism, in its turn, is as follows: SSFSP increases the corrosion resistance of AZ31B magnesium alloy due to change in the type of corrosion process. Instead of localized penetration in the form of pits, the stir zone undergoes the more uniform degradation in the form of distributed corrosion product. The idea is consistent with the previous literature on magnesium alloy corrosion and FSP [6,7,14,19].

The importance of the measured values is in their connection to each other. First, the surface texture determines the initiation sites; second, the refined microstructure determines the space for galvanic coupling; third, the polarization curve determines the rate of the process; and finally, post-corrosion morphology determines whether the attack will concentrate into pits or become distributed. Thus, it is possible to view the corrosion potential, polarization slope, grain size, and SEM morphological characteristics as sequential stages of the same mechanism, in which the low heat input produced by the stationary shoulder leads to microstructural modification and changes the continuity of corrosive paths.

2. Materials and Methods

2.1. Material, tool configuration, and processing condition

The study focuses on commercial AZ31B magnesium alloy plate with a thickness of 6.35 mm. It is noted that AZ31B Mg alloy was processed through a custom-designed H13 steel tool with a combination of a large static shoulder and a smaller rotating threaded probe. Single-pass FSS technique was conducted along the rolling direction of the base material with the help of a rotation rate of 700 rpm and a traverse speed of 100 mm/min. The static shoulder helps restrict movement of the material surface to minimize shoulder-induced thermal load while the rotating probe acts on the material as the primary source of localized plastic working. Optical and digital microscopy was utilized to examine the surface of the modified area while a cross-section analysis helped define stir zone, thermo-mechanically affected zone, and heat-affected zone [21].

Such a processing condition is metallurgically significant. A relatively thick magnesium alloy may generate considerable thermal asymmetry with respect to depth if the surface undergoes overheating via a conventional rotating shoulder. In case of a static shoulder, the degree of probe-based plastic strain is increased while the occurrence of surface flash, corrugations, and overheating is minimized. The surface topography analysis showed that there is no excess flash at all; the roughness variation is estimated at 50–100 µm. Such information is critical as any surface defect may attract electrolyte and serve as a nucleation site for corrosion initiation.

The first three figures of images show the processing environment of the sample used in the corrosion study. Figure 1 depicts the non-rotating shoulder during processing, while Figure 2 represents the processed area and the track indicating the test region for corrosion studies. Figure 3 provides an insight into the base material, thermo-mechanical affect zone, and stir zone present in the processed cross-section. Thus, based on the images presented above, the processing technique can be interpreted such that the corrosion resistance is analyzed on a surface generated by probe dominated deformation instead of a mechanically polished base material.

The depiction of the processing scheme in Figure 1 presents the non-rotating shoulder, rotating probe, direction of travel, and the resulting zonal microstructure created after processing. The most significant characteristic of SSFSP is the distinction made between

the shoulder responsible for determining the boundary condition of the surface and the probe causing the deformation. Due to this distinction, SSFSP makes it possible to create a stir zone of very fine dimensions without the necessity of imparting high surface thermal energy like the conventional rotational shoulder processing scheme. From the perspective of corrosion, the processing technique makes sure that the surface is not a mechanically polished base material, but the product of probe deformation.

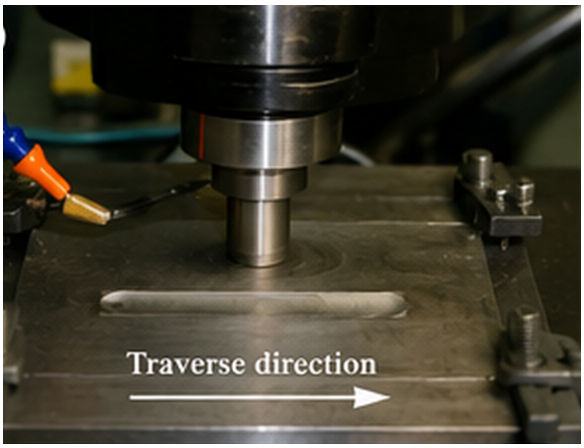

Figure 1. Tool contact during SSFSP.

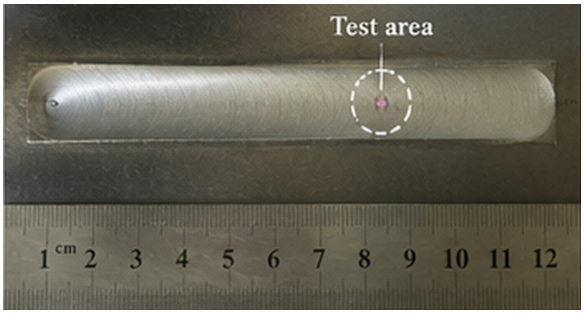

Figure 2. Processed track and test area.

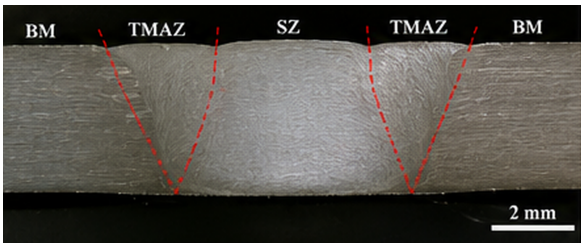

Figure 3. Transverse section with processed zones.

2.2. Characterization of Microstructure and its basis on grain size

The microstructural characterization was done through transverse sectioning and subsequent grinding, polishing, and etching with acetic solution. The stir zone grain sizes were measured at top, middle, and bottom areas of the stir zone in order to determine whether grain size is uniform in the depth direction. The average grain size of the base material is 25.2 ± 2.2 µm, while that of the stir zone is 6.34 ± 0.12 µm. From the small variance of the stir-zone grain size, one can infer that the material processed by stir casting is not only refined at the top but refined uniformly through out the processed layer. This is important since corrosion measurement is taken at the surface level, but corrosion resistance requires the underlying microstructure to be homogenously refined as well.

Dynamic recrystallization plays a fundamental role in achieving such microstructure in the stir zone. Severe plastic deformation near the stirring probe leads to increased dislocation density, storing deformation energy in the process. With the application of thermal cycle, recrystallized grains are able to form at the stir zone. Under the conventional process where a large proportion of heat input comes from the shoulder, there is possibility of significant difference in thermal history between the top and bottom regions of the material being processed. This is however reduced under the current SSFSP process due to low heat input at the bottom region.

The metallographic progression of Figures 4-9 ties the grain fields seen to the grain-size measurement reduction. The coarse base material field in Figure 4 is set against three fields of refined grains in the stir zones of Figures 5-7. The grain size comparison in Figure 8 confirms the reduction from 25.2 ± 2.2 to 6.34 ± 0.12 µm, and the depth-wise profile in Figure 9 confirms that the region of interest is not only finer, but uniform.

Figure 4. Base-material grain field.

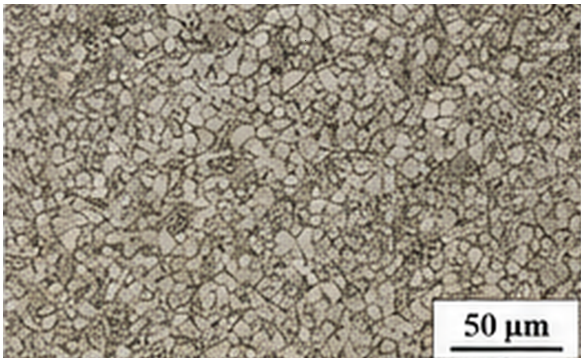

Figure 5. Refined stir-zone grain field I.

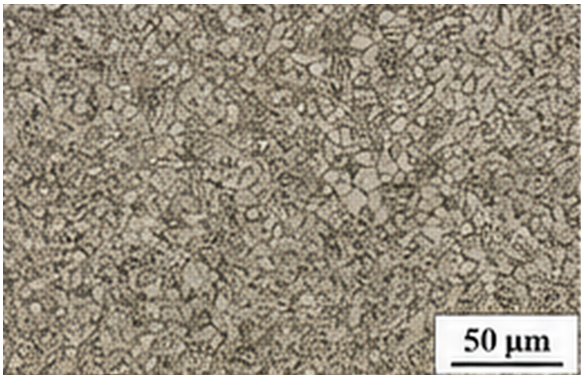

Figure 6. Refined stir-zone grain field II.

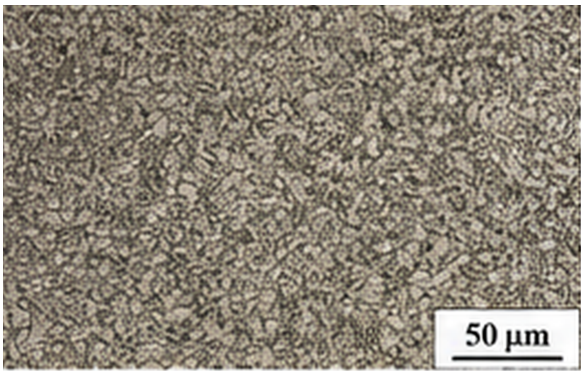

Figure 7. Refined stir-zone grain field III.

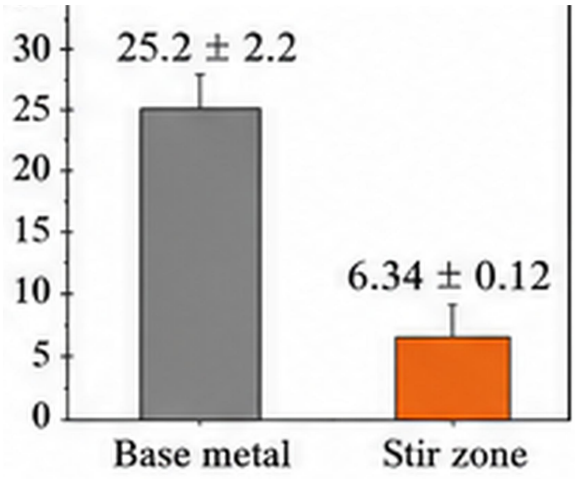

Figure 8. Measured grain-size reduction.

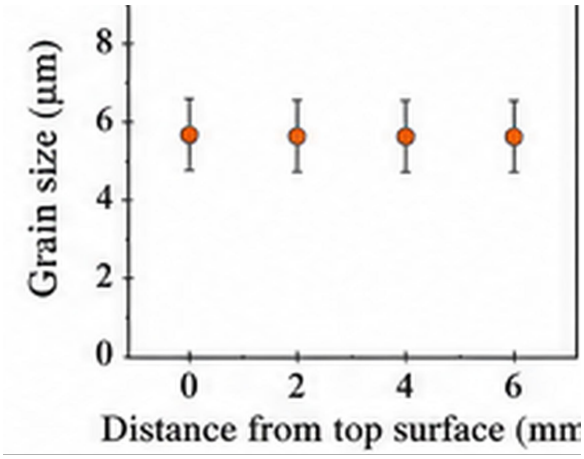

Figure 9. Depth-wise grain-size profile.

In this way, the measured comparison of Figure 8 and grain fields in Figures 4-7 show the change from coarse grains in the base material to refined grains in the stir zone. The comparison between these grain-size measurements shows a reduction in grain size, rather than a mere change in appearance. A reduction in grain size from 25.2 to 6.34 µm will increase the area of grain boundary per unit volume. While this could provide benefit in the case of magnesium by preventing corrosion front propagation along the grain boundary and by reducing segregation effects, this might work against the alloy in question if the grain boundaries were used by the reaction at anode sites.

2.3. Electrochemical analysis protocol

Electrochemical tests were performed on both the top surface of the substrate alloy and the stir zone. Prior to electrochemical tests, the surfaces were mechanically polished and cleaned with methanol. The electrolyte was a still and unde-aerated 3.5 wt% NaCl aqueous solution at ambient temperature. A three-electrode cell was employed, wherein the tested material served as a working electrode, saturated calomel as a reference electrode, and platinum served as an auxiliary one. The working electrode exposed surface area was 0.19625 cm^2, and each specimen was immersed in the electrolyte for 30 minutes prior to the electrochemical test. This was needed in order to achieve a steady potential. Open-circuit potential values were recorded, followed by potentiodynamic polarization scans in the range between −1.5 and +0.5 V versus OCP, with a scan rate of 2 mV/s. Corrosion potential and current density were calculated via Tafel extrapolation [21].

Under the aforementioned conditions, it would be justified to compare the corrosion behavior of the surfaces, since the electrolyte, area exposed to the electrolyte, reference electrode, scan range and preimmersion period have been kept the same. However, the method should be considered an accelerated test, which does not directly correlate with the service life of materials under consideration. Magnesium alloys may exhibit a different response due to the following reasons: the film rupture mechanism, hydrogen evolution, alkalinity of electrolyte, and time-dependent properties of corrosion products. Therefore, a reduced fitted corrosion current density would only be valid if accompanied with surface evidence of less severe localization. This is why the SEM morphology and EDS results are considered as core evidence and not as secondary visuals.

The cell arrangement in Figure 10, the exposed circular area in Figure 11, and the acquisition station in Figure 12 clarify the experimental geometry used for the electrochemical comparison. The same electrolyte, reference-electrode basis, exposed-area concept, and working-electrode configuration were applied to the base material and stir-zone surfaces, so the subsequent current-density contrast is not a consequence of a change in cell layout or measurement connection.

This experimental setup, as shown in Table 1, is crucial since it ensures that the corrosion test will not be separated from its real processing history and analysis process. The NaCl concentration and electrode configuration are kept constant for both the treated and untreated surfaces, and hence the high value of change in current density is not due to any difference in electrolyte concentration and area. Moreover, the process conditions represent a low heat input situation rather than an undefined one, since FSP, submerged FSP, and SSFSP all have the ability to refine grains in Mg-based materials, each having a unique flow path of energy and deformation process [12,13,18].

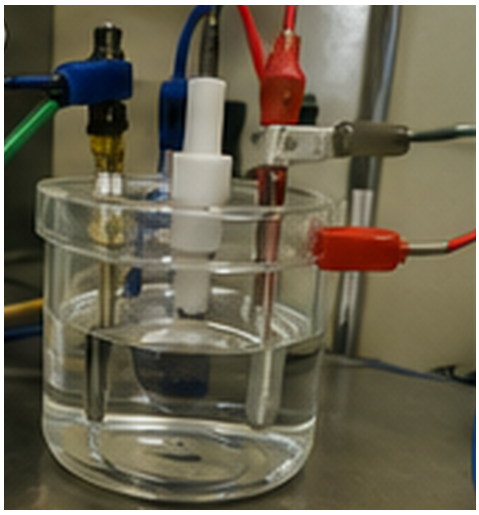

Figure 10. Electrochemical corrosion cell.

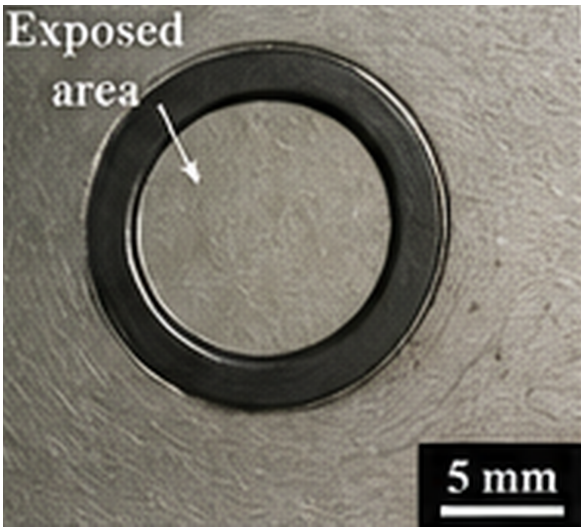

Figure 11. Exposed electrochemical area.

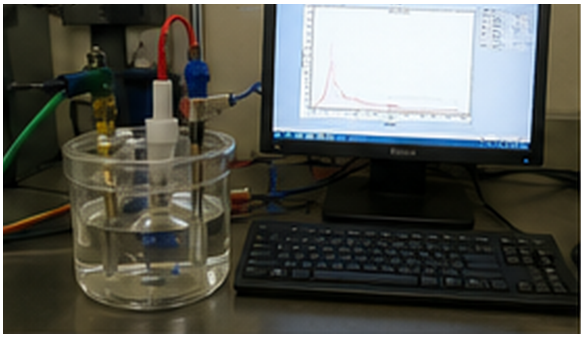

Figure 12. Cell and acquisition station.

Table 1. Experimental basis.

Parameter	Specific condition used for interpretation
Material	Commercial AZ31B magnesium alloy plate
Plate thickness	6.35 mm
Tool material and design	H13 steel system with stationary shoulder and rotating threaded probe
Processing condition	Single pass at 700 rpm and 100 mm/min along the rolling direction
Microstructural locations	Top, middle, and bottom of stir zone, with base-material comparison
Electrolyte	Non-deaerated, unstirred 3.5 wt% NaCl aqueous solution at ambient temperature
Electrode configuration	Working specimen, saturated calomel reference electrode, and platinum counter electrode
Exposed area and timing	0.19625 cm^2 exposed area, 1 h corrosion test, and approximately 30 min pre-immersion
Polarization scan	−1.5 to +0.5 V versus OCP at 2 mV/s
Post-corrosion examination	SEM morphology and EDS point analysis of base material and stir zone surfaces

2.4. Quantitative assessment of grain size reduction and current density changes

Three direct quantities were evaluated based on the results obtained. The reduction of the grain size was taken as

$$R_g = \left(1 - \frac{d_{SZ}}{d_{BM}}\right) \times 100, \tag{1}$$

where d_{BM} and d_{SZ} are the mean grain sizes of the base material and stir zone. The inverse grain-size ratio was defined as

$$G_i = \frac{d_{BM}}{d_{SZ}}, \tag{2}$$

which provides a simple relative indicator of the increase in grain-boundary density. The current-density reduction was defined as

$$R_i = \left(1 - \frac{i_{corr,SZ}}{i_{corr,BM}}\right) \times 100. \quad (3)$$

These expressions are purposely clear. The formulas are not meant to model electrochemistry; however, they serve the purpose of enabling comparison of the extent of microstructural improvement alongside the degree of corrosion-current diminishment in a comparable interpretive system.

Morphological evaluation was performed along similar lines. Pit density, intergranular structures, mud crack formation, and corrosion products were studied for the base material surface. These same aspects were evaluated for the stir zone surface, with an emphasis on identifying whether the pit formation was prevented or if pits were merely covered up by the corrosion product layer. In other words, the interpretation is not based on a single quantitative indicator only. A surface can have more fine cracks under the corrosion product film, yet be less hazardous than the one with fewer pits that penetrate deep into the substrate. Such distinctions are important for magnesium corrosion. The difference is significant to magnesium corrosion since local penetration affects the reliability of components more than general discoloration of the surface.

3. Results and Discussion

3.1. Effects of surface condition and low heat input processing strategy

The resultant surface exhibited minimal flash with low surface roughness values and arc corrugation. Such results are expected considering the function of the stationary shoulder as a wiping tool and not as a major source of frictional heat on the workpiece. The approximate surface roughness value of between 50 and 100 µm is an indication that the processing technique was not exposed to severe topographical variations normally associated with shoulder actions. However, surface smoothness is important from other perspectives. In the case of chloride corrosion, local electrolyte stagnation can occur in crevices, ridges, rough flash, and surface steps. Consequently, an increase in surface smoothness will reduce extrinsic initiation sites prior to consideration of the effects of the microstructure.

Low heat input is a critical issue in corrosion resistance. As seen in the cross-sectional profile of the sample, SSFSP resulted in a stir zone dominated by probe action and not the thermal footprint associated with FSP shoulder action. The equiaxed grains in the stir zone were consistent in size regardless of the location (top, middle, and bottom). The consistency of grain structure throughout the stirred layer is crucial since a potential through-thickness microstructural gradient in localized corrosion may facilitate pit penetration into a narrow zone along its depth.

The above observations point to how the processing strategy influences resistance to corrosion. The first mechanism involves the limitation of surface roughness due to the use of a stationary shoulder to limit the surface roughness and flash. In the second scenario, the reduction of the thermal gradient will ensure that the stir zone consists of fine-grained materials. While the two mechanisms address two distinct processes in corrosion, i.e., initiation and propagation, the resulting effect is a consequence of a fundamental shift in the near-surface corrosion environment.

3.2. Grain refinement and corrosion implications thereof

Grain size variation would be the most direct effect on the microstructure. The base metal had grains of size 25.2 ± 2.2 µm, while the stir zone had grains of size 6.34 ± 0.12 µm. This indicates that there was a decrease in grain size by 74.84% and an inverse increase in grain size by 3.97. It is also important that there was a much lower standard deviation of the stir zone grain size since this would indicate smaller variance of the microstructure size

scale. Even in a highly refined yet inhomogeneous region, localized corrosion may occur due to coarse areas.

The numerical quantification provided in Table 2 indicates that the effects on microstructure and electrochemistry have comparable magnitudes. While the refinement in grain size was nearly 75%, the corresponding reduction in current density was almost 79%. This correlation between parameters cannot serve as direct proof of a cause-and-effect relationship, but the fact speaks for the controlling nature of the structural modification in the context of enhanced corrosion resistance rather than the trivial surface treatment. The very small change in the corrosion potential is also significant from this point of view. It shows that there was no pronounced shift in the thermodynamic tendency towards corrosion. Instead, the effect was based on changes in the kinetics and morphology of corrosion.

Table 2. Measured and calculated changes.

Descriptor	Base material	Stir zone	Interpretation
Mean grain size	25.2 ± 2.2 μm	6.34 ± 0.12 μm	74.84% reduction after SSFSP
Inverse grain-size ratio	1.00	3.97	Higher relative grain-boundary density in the stir zone
OCP trend	about -0.65 to -0.47 V	about -0.40 to -0.35 V	More stable and nobler open-circuit band in the stir zone
Corrosion potential	approximately -0.546 V	approximately -0.546 V	Similar fitted potential despite different morphology
Corrosion current density	9.815×10^{-3} A/cm^2	2.032×10^{-3} A/cm^2	79.30% reduction after SSFSP
Dominant corrosion morphology	Deep pits, mud cracking, and intergranular attack	Corrosion-product film, limited mud cracking, and no comparable deep pits	Change from localized attack to more distributed surface degradation

This approach requires special attention to the possible role of grain boundaries. They can be regarded as preferential sites for localized corrosion, especially in cases when segregated solutes form within grain boundaries or the contrast between the two adjacent grains (cathode/anode) is pronounced. On the contrary, a uniform grain structure with small grain sizes encourages the development of stable oxide film and prevents the formation of local cells. The data clearly indicate the latter case as the grain refinement resulted in decreased current density and better morphology of pits. This conclusion is also consistent with the literature discussing the improvement of magnesium corrosion properties after FSP via refining and homogenizing grain structure [6,7,14].

Finally, it is worth noting that the relatively small variation of the grain size in the stir zone is critical. Traditionally, the FSP process can lead to non-uniformity in terms of the grain structure, with smaller grains formed close to the shoulder due to increased heat input and larger grains located deeper into the stir zone. In cases when the gradient was quite high, the process of corrosion may start from the surface but evolve with interaction with a constantly changing subsurface structure. The stationary shoulder significantly diminishes this problem and enables the formation of a relatively uniform microstructure during the rotation of the probe.

3.3. Open-circuit potential and polarizability behavior

The open circuit potential measurements clearly differentiate the base material from the stir zone prior to potentiodynamic polarization. The stir zone showed relatively stable values of around -0.40 to -0.35 V while the base material showed instability varying between -0.65 and -0.47 V in the electrochemical test. An OCP showing stability implies better consistency in the relationship between the dissolution and cathodic activities on the surface. For magnesium alloys, an unstable open circuit potential could be due to the active formation of protective films, protective film breakdown, variation in cathode size, or changes in local chemistry on the surface.

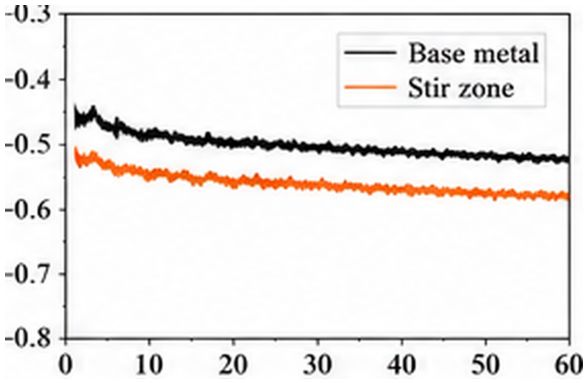

Figure 13. Open-circuit potential response.

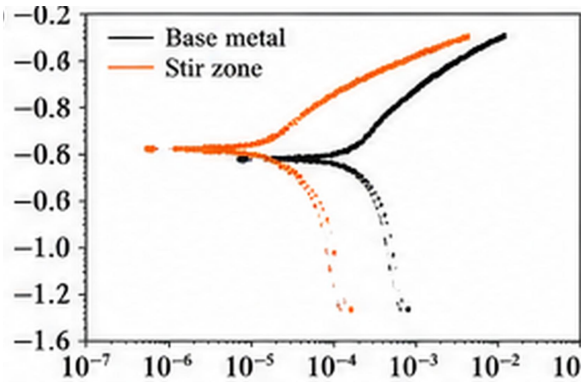

Figure 14. Potentiodynamic polarization.

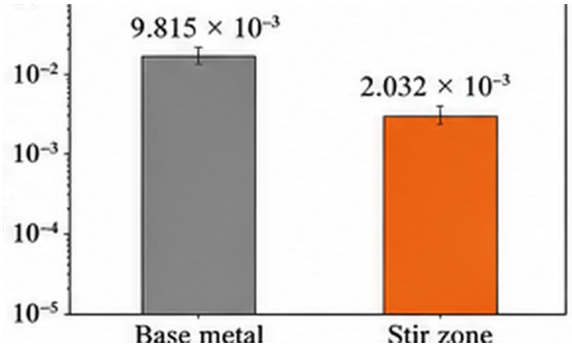

Figure 15. Corrosion-current comparison.

It is worth noting the division between the electrochemical panels in Figures 13 and 15, between potential stability and kinetics respectively. In Figure 13, the OCP behavior of the base material provides the wider base-material trend, while the stir-zone OCP gives the narrower stable stir-zone trend. The polarization curves in Figure 14 confirm the comparable corrosion potentials for the two samples, while the bar comparison in Figure 15 quantifies the difference in terms of reduced current density: 9.815×10^{-3} to 2.032×10^{-3} A/cm^2, which amounts to a reduction of 79.30%.

The electrochemical response curve in Figure 14 confirms that although the fitted corrosion potentials for the two samples are comparable, their corrosion current densities differ substantially. Both of these pieces of information combined provide insight into the mechanism of the difference. While the first piece alone suggests that the two materials are similar, the second piece reveals that there is in fact significant kinetic difference: that is, the corrosion potential for the stir-zone surface represents a much slower reaction rate. The actual measured difference of current densities, namely a decrease from 9.815×10^{-3} to

2.032×10^{-3} A/cm^2, represents a 79.30% reduction, or an improvement factor of ~ 4.83 if compared as a ratio ($i_{corr,BM}/i_{corr,SZ}$).

Polarization curve must be discussed alongside with the open-circuit behavior of the base material, rather than separately from it. Stir zone has a lower OCP value, which means that when it starts its response, it is starting from a more stable OCP state, and then it maintains a lower current density throughout the polarization process. Base material has a higher OCP value, which means that it starts from an even more active and drifting OCP state, and then generates a higher current density. All of these pieces of information are consistent with each other. Base material is not just more reactive in terms of polarization under scanning applied potential; it was already less stable under open-circuit conditions.

The existence of a similar corrosion potential near -0.546 V also contributes to the clarification of this effect. The stationary shoulder process did not convert AZ31B to a different alloy; it was not converted to a different phase with an entirely new tendency toward equilibrium. The alloy composition remains AZ31B; the electrolyte remains chloride solution. The difference is not in the overall chemical composition or equilibrium properties but in how the reactions occur. The processing strategy may have achieved an improvement through changing the pattern of the reaction and making localized cells easier or harder to form [22,23].

3.4. Base-material corrosion morphology

In this context, the morphological image of base-material corrosion can be seen as an explanation of the open-circuit instability and the higher current density in the polarization curve. Localized pitting is the most obvious feature present in the surface morphology of base-material corrosion. Enlarged regions show additional features such as mud cracking and intergranular paths. These types of morphology are characteristic of the corrosion mode that involves localized pitting. Pits imply that the corrosion reactions did not progress evenly across the exposed surface; they were instead concentrated at some particular areas. Once formed, the pits create their own microenvironment in which acidification, enrichment with chloride, and film disruption sustain the corrosion process.

Base-material samples provide clear insight into why a higher current density is significant. Figure 16 illustrates uneven corrosion-product formation on the exposed surface, while a pitting overview in Figure 17 confirms strongly penetrated corrosion field. A cracked product in Figure 18, as well as high magnification in Figure 19, demonstrates the dangerous localization mode, while Figure 20 presents oxygen-, magnesium-, aluminum-, chloride-, and zinc-containing corrosion products at the tested area. Thus, morphological and EDS findings support the claim that the base material is susceptible to localized attack rather than general oxidation process.

It is important to note that a high current density alone does not completely characterize the situation. Naturally, it can be assumed that the observed current density is associated with surface activity and thus corrosion processes, but the type of surface geometry controls the degree of threat. Pits and inter-grain structures significantly increase the rate of corrosion and make the structure susceptible to crack formation much sooner than a simple corrosion layer could do it. Therefore, the analysis suggests that the base material is prone to localization. Numerous pits, cracks, and mud-cracked products point to an active formation of new layers of oxide film on a regular basis.

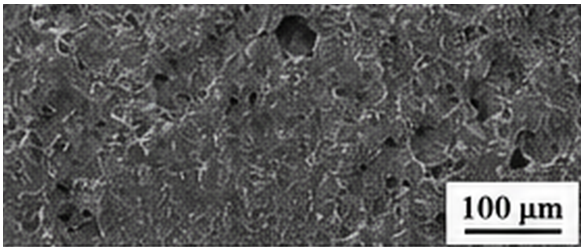

Figure 16. Base-material corroded overview.

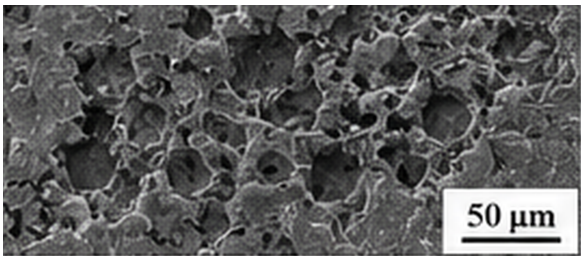

Figure 17. Base-material pitted surface.

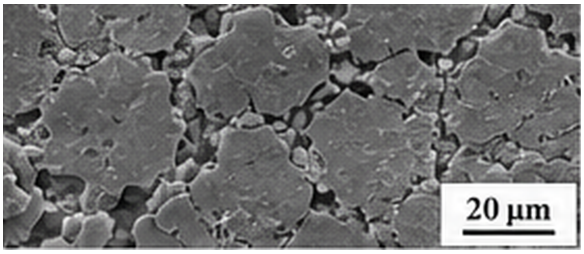

Figure 18. Base-material cracked product.

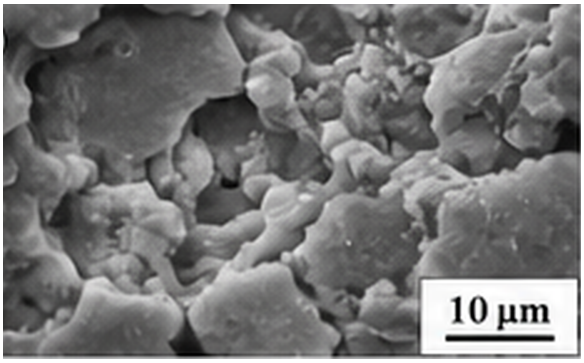

Figure 19. Base-material high-magnification morphology.

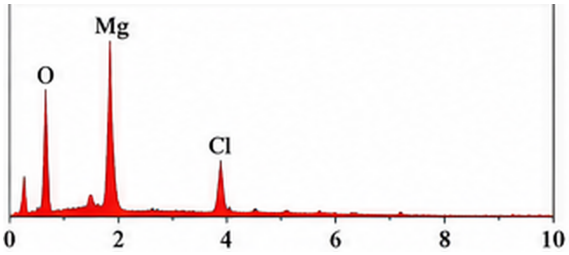

Figure 20. Base-material EDS spectrum.

EDS data gathered from corroded areas supports the proposed micro-galvanic hypothesis. As previously mentioned, AZ31B includes some basic alloying elements such as Al and Zn. Aluminum–manganese–iron particles can be responsible for local corrosion as these particles can be considered cathodic in relation to the alpha-Mg phase. In case of base materials, their continuity and bigger grain size ensure greater cell activity over a longer distance. Such a conclusion is consistent with past research on magnesium corrosion suggesting that localized corrosion can be accelerated due to the presence of alloying elements and impurities [2,3,24].

Mud cracks appearing on the base material sample should not be considered a neutral phenomenon. Generally, mud cracks are formed during a corrosion of brittle or dried layers. The appearance of mud cracks means that the film is not able to stabilize itself. Indeed, its

mechanical properties fail under the impact of growing stresses and changing volume. If this kind of cracking is combined with inter-grain paths and pit formation, electrolyte will have easy access to magnesium metal. In this way, there appears a feedback loop. Cracks open, revealing new magnesium, corrosion continues, creating more products and stress.

3.5. Corrosion features of the stir zone

In the stir zone, there is an entirely different pattern of corrosion. As observed by SEM, there is extensive coverage of the corroded product on the sample surface, with only a few places where mud cracks occur, without the presence of deep pits, like those found in the base material. However, this is not because the stir zone does not corrode. Corrosion still occurs in the stir zone since magnesium is still reactive in NaCl solution.

The stir-zone surfaces shown in Figures 21–23 demonstrate a distinct morphology compared to the base metal. While the overview image in Figure 21 shows a large coverage of corrosion product, images in Figure 22 and 23 indicate cracked corrosion products and deposits without the population of deep pits seen in the base metal samples. The morphology indicates that SSFSP changes the mode of corrosion from localized attack to film-type corrosion. This differentiation is important since the corrosion process persists in the stir zone but becomes less localized.

The microstructure in Figure 21 provides the morphological correlate to the decrease in i_{corr}. Lowering the current density can be theoretically possible despite the remaining corrosive attack being located in several critical locations. This is not the case here since the lack of deep pits and the more even distribution of corrosion products suggest that SSFSP changes the geometry of the corrosion process. The lower current density thus goes hand in hand with a less localized corrosive attack pattern.

Such change can be explained by the refinement and homogeneity introduced by SSFSP. The fine equiaxial structure leads to smaller distances between boundaries, while the SSFSP process allows dissolving or mechanically disrupting Al–Mn–Fe clusters that can increase localized galvanic potential difference. With clusters dissolved, the cathodic and anodic sites become less likely to form aggressive pairs of cells. Therefore, the corrosion will take place in a wider area, making deep pits unlikely. This phenomenon was already observed in previous studies of FSP, where refinement and homogeneity led to increased corrosion resistance, as well as the contrary trend in bimodal microstructures [6,7,14].

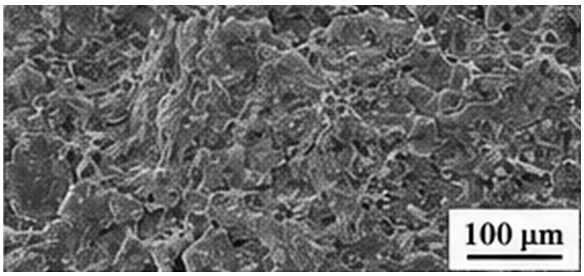

Figure 21. Stir-zone corroded overview.

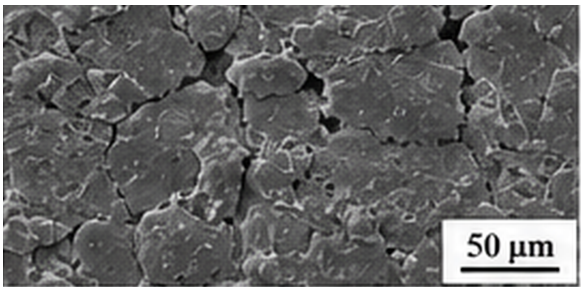

Figure 22. Stir-zone cracked product surface.

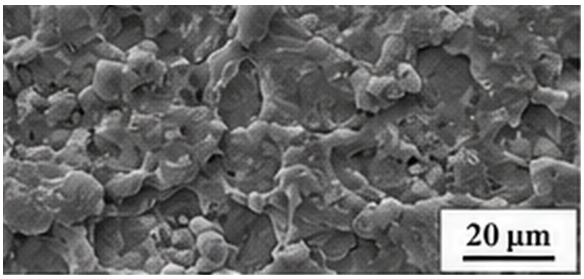

Figure 23. Stir-zone high-magnification product.

Mud cracks in stir-zone surfaces need to be considered separately, as mud cracks appear in both cases. However, while the base metal sample shows numerous mud cracks in the vicinity of deep pits, the stir zone exhibits mud cracks on only part of its surface within corrosion products. The presence of mud cracks indicates different levels of severity, rather than two distinct features, depending on other characteristics of the sample morphology. Interpreting mud cracks as equally severe would ignore the true mechanism of the observed effects.

In addition, the stir-zone pattern explains why surface processing can be useful even without introducing a different alloy composition. Neither the stir zone nor any other FSP treatment creates additional coating protection or a new alloy layer. By refining the microstructure and making it more homogeneous, the surface process can modify the native corrosion process. This modification is important when it comes to applications where the coating can be easily removed or a surface that should corrode but not penetrate too aggressively is needed.

3.6. Transformation in corrosion modes and significance of current densities

The combined findings from the electrochemical and morphological tests suggest a change from localized to more generalized corrosion. The substrate metal exhibits higher corrosion current density, unstable pattern of OCP, presence of many pits, inter-granular structures, and abundant mud cracking. The stirring zone exhibits lower corrosion current density, stable band of OCP, large coverage with corrosion products, few mud cracks, and absence of equivalent pits. The main finding from these tests is not that there is no corrosion in the stirring zone. It is rather that corrosion modes transform from localized to generalized corrosion.

The comparative sequence in Figures 24–29 clearly highlights the transition. Specifically, the overview comparative sequence in Figure 24 highlights the differences between the base material surface and the processed stir zone surface. In terms of close-up views, Figures 25 and 26 demonstrate the role of pit/intergranular corrosion in the base material and that of the distributed product layer in the stir zone. Product cracking and damage textures are compared side-by-side in Figures 27 and 28, respectively. The montage sequence in Figure 29 combines cross-section, grain refinement, OCP measurement, and corrosion mode into one evidence chain.

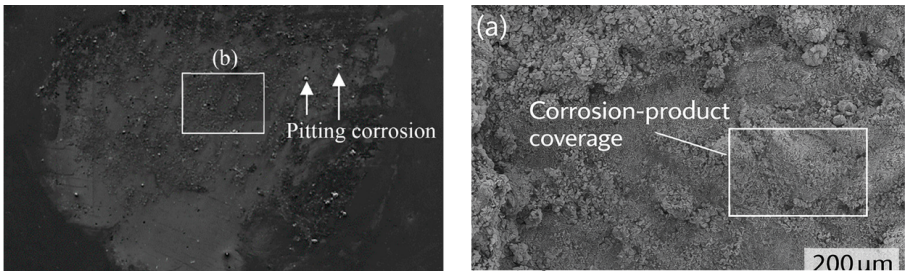

Figure 24. Base-material and stir-zone overview pair.

The summary for the transition in Figure 29 clearly differentiates between rate and damage morphology. While the base material suffers from coarse microstructure and

localized cells for initiating pits, the stir zone benefits from dynamic recrystallization and particles disruption that favor distributed product deposition in addition to thermal symmetry. The product may suffer damage cracks, yet there is no alignment between the damage cracks and pits as the latter tend to form deeper in the base material. Thus, the material is subject to both lower current density and less hazardous damage morphology.

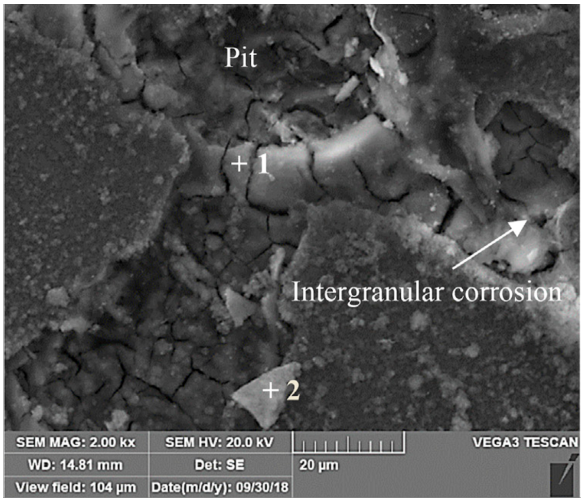

Figure 25. Localized base-material pit region.

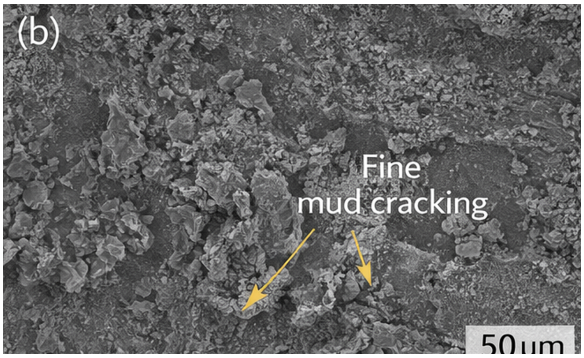

Figure 26. Distributed stir-zone product region.

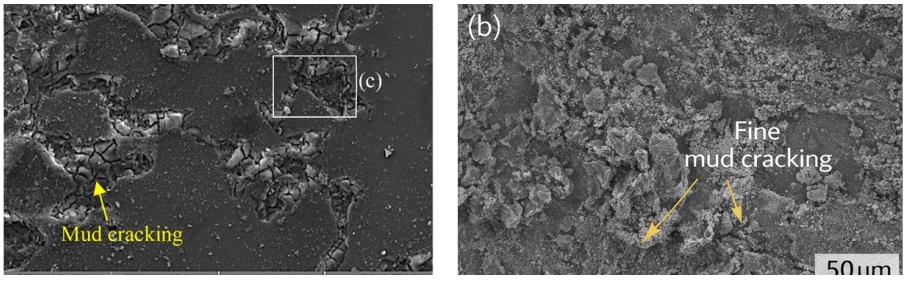

Figure 27. Mud-crack morphology pair.

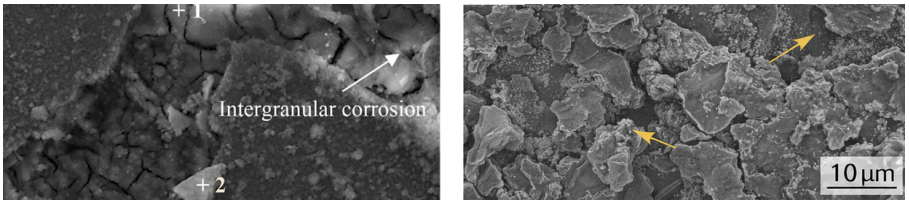

Figure 28. High-magnification damage pair.

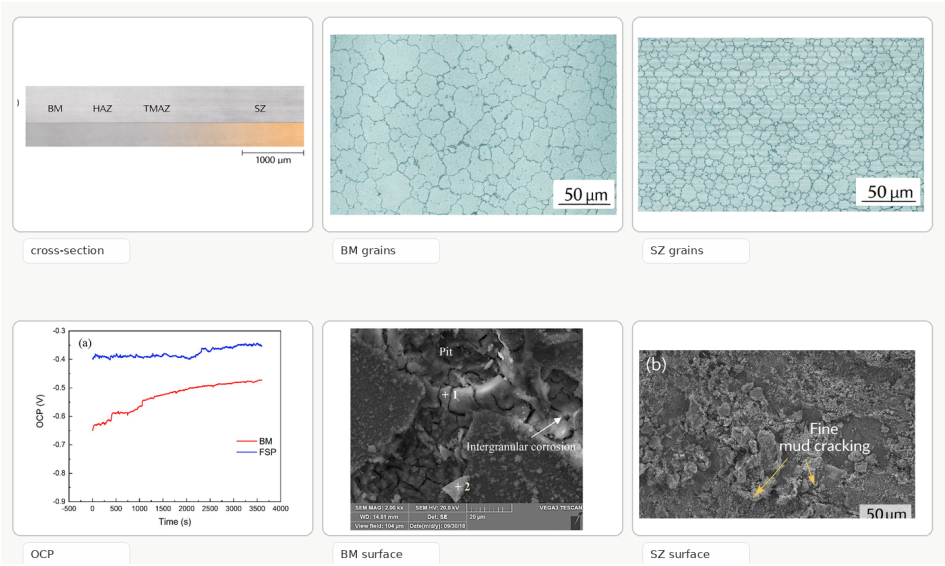

Figure 29. Integrated evidence montage.

An effective way to characterize the result obtained in this work involves separating corrosion intensity and corrosion localization. The former term denotes the intensity of the electrochemical reaction, which in turn is indicated by i_{corr} here. On the other hand, the latter term describes the degree of concentration in electrochemical activity, which can be characterized by pits, pathways, and heterogeneity in corrosion product distribution. As such, the base material is characterized by high intensity and high localization; whereas, the stir zone exhibits low intensity and low localization in its corrosion characteristics.

The independent evidence presented in Table 3 demonstrates that the conclusion remains valid based on different lines of observation. Electrochemistry suggests the presence of a slower reaction rate in the stir zone. Microstructure suggests a refined and uniform grain structure. Morphology suggests a different corrosion mode. Since all three forms of evidence are consistent with one another, the conclusion cannot rely on misinterpretation of a single figure or parameter value. This reinforces the general hypothesis that stationary-shoulder processing reduces localized corrosion in AZ31B by altering its microstructural foundation.

Table 3. Evidence for corrosion-mode change.

Evidence category	Base material response	Stir-zone response
Open-circuit behavior	Broad drift from about -0.65 to -0.47 V	Stable band near -0.40 to -0.35 V
Polarization	Higher i_{corr} of 9.815×10^{-3} A/cm^2	Lower i_{corr} of 2.032×10^{-3} A/cm^2
Grain structure	Coarser grains of 25.2 ± 2.2 μm	Fine equiaxed grains of 6.34 ± 0.12 μm
Localized attack	Large number of pits and intergranular features	No comparable deep-pit population
Corrosion products	Mud cracking associated with localized attack	More distributed surface film with limited mud cracking
Mechanistic implication	Connected micro-galvanic paths promote concentrated dissolution	Homogenization and particle disruption weaken localized galvanic propagation

The fitted corrosion potential merits particular consideration since it helps avoid overly simplistic interpretations. Both surfaces show similar E_{corr}, but there are large differences between their i_{corr} and morphological characteristics. In electrochemistry, it is possible to see similar mixed potentials despite differences in active area, cathodic efficiency, and local transport properties. From a physical perspective, a surface will corrode with a lower overall rate and different geometry without a substantial displacement of the fitted corrosion potential. That is why it is essential to interpret a polarization curve with morphological evidence.

This aspect bears specific importance for reviewer considerations since magnesium alloy corrosion studies tend to overestimate the significance of corrosion potential. A nobler

corrosion potential can be helpful, but it does not equal good corrosion resistance if localized initiation and propagation processes continue. This argument is further strengthened by the correlation between the decrease in corrosion rate and the reduction of deep-pit morphology. In this way, the conclusion is built upon convergent evidence and not just a single electrochemical parameter.

The transformation in the corrosion mode adds further support to the notion that SSFSP is more than an alternative configuration for FSP tools. The rotating shoulder can create considerable plasticization on the surface, but it might also lead to overheating or excessive surface corrugation. The stationary shoulder makes it possible to achieve dominant plasticization by the probe while maintaining surface constraining by the shoulder. In case of thick AZ31B, this leads to smoother and more uniform surface refinement in the stir zone. Thus, the corrosion effect is achieved due to the full processing process architecture.

3.7. Fracture-like surface features and image-based interpretation

Irregular cracks, pits, and corrosion product film boundaries complicate the description of morphology of magnesium alloy corrosion using traditional scalar metrics. This can be addressed with the aid of image-based analysis as long as the selected descriptor reflects physical objects. The box counting approach has been adopted for corrosion analysis due to its ability to reflect fractal boundaries and crack networks' scale-dependent space-filling behavior [25–28]. From the standpoint of the present study, the crack network descriptor is meaningful only in the framework of simultaneous consideration with the electrochemical rate and corrosion mode.

The crack network panels in Figures 30-35 show how image descriptors need to be read together with morphology, rather than as a severity measure in its own right. Figure 31 gives the mask and ROI for a crack network formed by pit-dominated corrosion, and Figure 32 shows the fitted curve for its scaling properties. Figure 33 is the corresponding ROI for a less localized corrosion-product network. Figure 34 is the corresponding mask, and Figure 35 gives the fitted curve for scaling. This contrast supports the paper's view that increased spatial complexity of a product film does not imply increased or more dangerous corrosion damage.

The image analysis in Figure 30 shows a critical issue. A more complex-looking network of cracks in a corrosion product does not necessarily indicate more serious attack. A distributed corrosion film can create numerous fine cracks, thereby covering more pixels of an image. Meanwhile, base material will have relatively few segmented cracks but deeper and more destructive pits. Thus, fractal or box-counting analyses should not serve as a sole indicator of corrosion severity. Rather, these methods only classify spatial pattern. Penetration depth, chemistry, and mechanical effects of pitting have to be assessed separately.

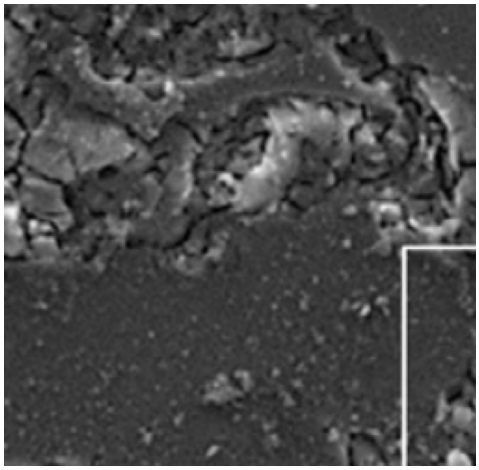

Figure 30. Base-material corrosion ROI.

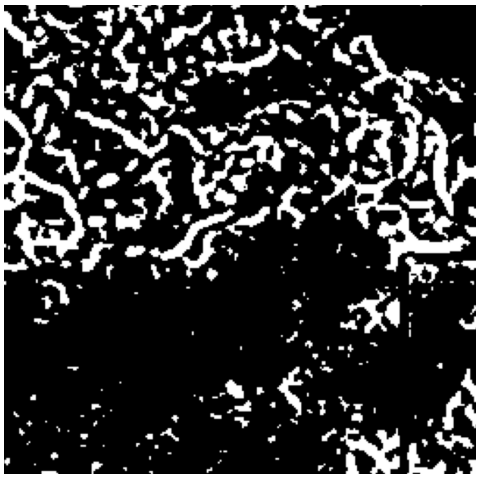

Figure 31. Base-material crack mask.

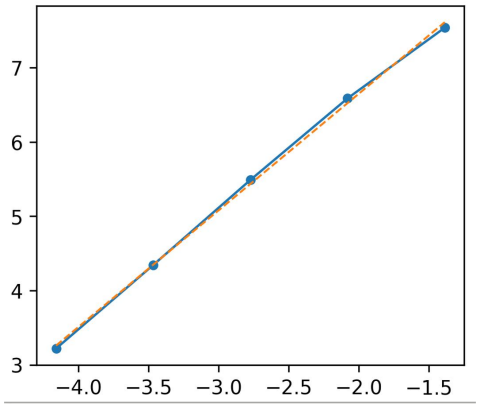

Figure 32. Base-material box-count fit.

Figure 33. Stir-zone corrosion ROI.

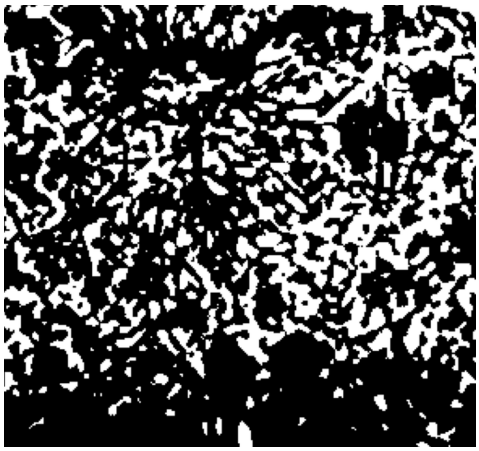

Figure 34. Stir-zone crack mask.

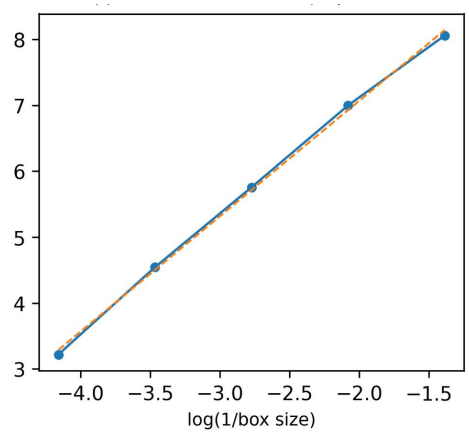

Figure 35. Stir-zone box-count fit.

The physics becomes clearer once the crack network information is considered alongside the SEM observations. The base material is subjected to deeper pitting and intergranular corrosion. Therefore, this area will suffer from a more severe corrosion process regardless of a binary mask's lower space-filling properties. The stir zone will have a more evenly distributed corrosion product film. It means that the crack network in this case can appear highly complicated despite less localized attack. This issue highlights the main weakness of image analysis. A higher value of a complexity metric can reflect either a severe pitting event or a distributed corrosion film, depending on segmentation. Image analysis-based investigations have noted the above problem [29,30].

As shown, morphology and electrochemistry for AZ31B lead to the same conclusions. The base material is more severely affected by pitting and intergranular attack due to higher current density. Meanwhile, the stir zone exhibits less severe attack with lower current density and uniform corrosion. This is a typical example where the complexity metric does not provide reliable evidence about corrosion. Crack network analysis is therefore a complementary descriptor of corrosion geometry rather than a primary evidence of enhanced corrosion resistance.

3.8. Mechanistic synthesis

The observed effects can be interpreted as a result of sequential changes due to the process. First, SSFSP introduces intense plastic deformation using the rotating probe but minimizing the heat of friction from the stationary shoulder. Dynamic recrystallization occurs, leading to formation of an equiaxed fine grain stir zone. The lack of motion of the shoulder means the absence of frictional heat dissipation by sweeping along the surface;

thus, the surface gets smoothed, while the thermal gradient across the stir zone decreases. Homogeneity of the near-surface microstructure emerges as a result.

The second stage is change of the electrochemical characteristics. In the base material, larger grains and presence of Al-Mn-Fe particles facilitate formation of large galvanic cells, leading to dissolution of anodic zones and formation of deep pits. With SSFSP treatment, particle disruption, partial dissolution, and grain refinement lead to smaller sizes and fragmentation of galvanic cells. Though the reaction of electrolyte with alpha-Mg remains unchanged, the localization in space of the chemical process gets disrupted. As a consequence, smaller values of i_{corr} are achieved not merely due to fitting parameters but as a direct effect of change in electrochemical accessibility of reaction centers.

The third stage is morphology. Formation of pits, intergranular corrosion, and mud cracks is typical of the base material, whereas the stir zone is characterized by uniform coverage by corrosion products and mud cracks but absence of deep pits. Thus, the proposed scenario provides a reasonable interpretation of the observed trends.

This scenario explains why the corrosion potential remains constant while the corrosion currents and morphologies differ. The composition of the alloy is still magnesium-based, but its spatial organization gets changed.

This interpretation is consistent with, yet more specific than, a general claim about the effect of grain refinement. In particular, low heat input, through-thickness uniformity, particle disruption, and localization suppression are interacting factors leading to improved corrosion resistance. However, a grain refinement performed using some poor control of the process might not have the desired effect. For instance, AZ31 processed via FSP demonstrated a bimodal grain structure, which was linked to unfavorable corrosion characteristics. In addition, homogenized and refined AZ31 and AZ91 exhibited improved corrosion performance compared to the base materials [7,14]. In contrast, the presented case with SSFSP belongs to the former category because the improvement is accompanied by homogeneity of the stir zone.

The main practical advantage of the considered scenario is in reduction in spatial concentration of the localized corrosion. While a decrease in average corrosion rates is always desirable, the avoidance of penetration at a single point could be more important for a long lifetime of the part. This is why SSFSP represents an attractive processing approach because of effective suppression of deep pits without use of any protective layers or inhibitors. The same reasoning applies to biodegradable medical implants, where uniform erosion is preferred to localized one despite the necessity of complete degradation.

Thus, it is essential to realize that the process design in relation to corrosion characteristics should focus on the aspect of reliability. Although one can expect the best results with maximum grain refinement, other factors, including texture homogeneity, minimal stress concentration, and reduced concentration of cathodic particles, are also critical. On the contrary, the process condition leading to moderate grain refinement but high uniformity should be preferred. The proposed SSFSP condition can be judged as favorable because of consistency of processing characteristics, grain size distribution, OCP stability, reduction in current density, and morphological observations. The same logic applies to other magnesium alloys.

3.9. Relation to past studies on magnesium and FSP corrosion behavior

The findings of this study are consistent with various aspects of past literature about magnesium corrosion and FSP corrosion behavior. In classical studies, magnesium corrosion is attributed to instabilities in the corrosion product film and galvanic coupling, particularly in chloride-containing electrolytes [1,2,23]. Based on the base material morphology, the corrosion of Mg AZ91 alloy in this study could be characterized using the same terminology: pitting and intergranular corrosion. The increase in the current density is hence predictable for the larger and less homogeneous grains.

In terms of stir-zone behavior, the findings are consistent with studies in which FSP enhances corrosion resistance by refining the surface layer or redistributing second phases

[6,14]. The SSFSP study here offers a specific mechanism: the effect of the stationary shoulder on reducing thermal asymmetry and minimizing surface roughness. The uniformity of the refined microstructure contributes to an increased corrosion resistance at least at a certain stir-zone depth.

The findings are consistent with studies indicating the negative effect of FSP on magnesium corrosion as well. Saikrishna et al. indicated a reduction in the corrosion resistance of AZ31 Mg alloy due to the bimodal grain size distribution caused by FSP [7]. Similarly, Argade et al. observed that magnesium rare-earth alloys exhibited complex corrosion resistance depending on both alloy composition and microstructure [11]. Therefore, FSP cannot always be considered beneficial for the alloy's performance under all conditions. The improvement observed in the present study is a result of the specific processing state that leads to a uniform refined microstructure.

SSFSP literature provides the necessary manufacturing context. Earlier SSFSP studies proved that a stationary shoulder decreased heat input and promoted grain refinement, while the backing plate control studies revealed that the degree of heat dissipation was essential for the thickness-dependent refinement [18–20]. The results of corrosion behavior extend the manufacturing logic by adding the aspect of electrochemical performance. The key aspect in determining the corrosion behavior is not merely the grain refinement, but the ability of FSP to produce a homogeneous corrosion-resistive surface layer rather than a thermally-graded surface.

Fractal and box counting analysis brings yet another dimension to the comparison. These tools had been applied for decades to measure corrosion texture, but this study highlights the issue with these approaches. A surface with a large number of distributed fine cracks would exhibit a more complex fracture network despite the lower probability of local pits compared to one with fewer but deep local pits [26–28]. The difference is especially evident in magnesium alloys, in which corrosion products form cracks even in a uniform attack.

3.10. Significance of localized-corrosion suppression to engineering

While the suppression of deep local attack is valuable in its own right, the practical engineering value of the SSFSP condition should be understood as more than a quantitative reduction in current density. As a rule, magnesium alloy components fail reliably after rapid formation of a few pits because local geometric features create stresses, increase electrolyte retention, and reduce penetration times to perforation and cracking. In terms of the material morphology, this means that pits, intergranular corrosion, and cracks offer the necessary paths for chloride solution. In contrast, the stir zone morphology is characterized by a spatial distribution of corrosion products and lack of deep pits. Thus, the morphology of the SSFSP condition is more suitable for applications that depend on preventing local penetration.

The manufacturing aspect is also relevant to the significance of the SSFSP condition. By having the shoulder stationary, the tooling configuration allows avoiding surface heating, friction, and rubbing, which tend to generate undesirable phenomena such as flash, corrugations, and overgrown grains on the top surface. In the case of the 6.35 mm thick AZ31B plate analyzed above, the rotating threaded pin serves to deform the metal, whereas the non-rotating shoulder helps restrain the top surface. This functional distribution accounts for both the smoothness of the surface track and small size of grains within the stir zone. In turn, the corrosion resistance of the surface results from an integrated effect of limited roughness, small grain sizes (25.2 ± 2.2 vs. 6.34 ± 0.12 µm), and discontinuity of micro-galvanics due to particle dislocation.

In terms of the claim boundary, the examined condition provides sufficient basis to conclude that a single SSFSP pass at 700 rpm and 100 mm/min increases the corrosion resistance of the AZ31B alloy in non-deaerated 3.5 wt% NaCl solution. There is no need to specify an optimal rotational speed, traverse speed, shoulder geometry, immersion time, or salt concentration. Additional tests would help separate the contributions of film

resistance, charge transfer resistance, cathodic kinetics, and penetration depth, but they are unnecessary for answering the main question posed by this investigation, which has been done using the electrochemical data and SEM images. The latter show a significant decrease in deep pits, which account for the measured 79.30% reduction in i_{corr}.

From the perspective of the mechanism, the most appropriate interpretation is linked with the manufacturing process. In other words, the SSFSP condition contributes to increased corrosion resistance of the AZ31B alloy plate because it provides for a smooth, fine-grained, and homogeneous surface layer. This conclusion excludes such alternative interpretations as changes in the chemical composition of alloy, surface coatings, or shifts in corrosion potentials. Rather, the increased corrosion resistance is related to the morphological changes that occur after chloride exposure, namely, inhibition of localized attack leading to deep pits.

4. Conclusion

The research question is whether the stationary-shoulder friction stir processing (SSFSP) improves localized corrosion resistance of AZ31B magnesium alloy by switching the corrosion mode from pitting to uniform, or if it simply results in reduced polarization current. Based on the obtained results, it can be concluded that the former interpretation is correct, i.e., SSFSP yields a reduction both in the corrosion reaction rate and in its localized character. In the stir zone created in 6.35 mm thick plate with 700 rpm rotation speed and 100 mm/min travel velocity, the grain size of 6.34 ± 0.12 μm is formed, as opposed to 25.2 $\pm$ 2.2 μm in the base material. This means a 74.84% grain size reduction and an inverse grain size increase by 3.97 times.

According to electrochemical experiments performed in non-deaerated 3.5 wt% NaCl solution, the stir zone demonstrates significantly more stable open-circuit-potential band than the base material. The corrosion potential value calculated for both states is very close and equal to -0.546 V. On the contrary, the corrosion current density is much lower (2.032×10^{-3} A/cm^2 vs. 9.815×10^{-3} A/cm^2), thus being decreased by 79.30%. This fact testifies to the change in the kinetics and spatial pattern of the corrosion process rather than creation of any thermodynamic barriers to it.

The most conclusive information can be obtained by analyzing the micro-morphology of the corroded sample surfaces using SEM/EDS. The base material exhibits numerous signs of deep-pitted surface structure, mud cracking and intergranular corrosion, which are all characteristic of localized corrosion. The stir zone demonstrates a relatively uniform corrosion-product coverage with minimal mud cracking and absence of comparable deep pits. Corrosion products form in both cases, but their distribution and level differ greatly. As a result, the SSFSP alters corrosion from a pit-driven mechanism into a more distributed surface-film one.

The discussed changes are caused by several factors working simultaneously: low heat input, minimized through-thickness thermal asymmetry, dynamic recrystallization and grain refinement, weakening of micro-galvanic continuity due to dispersion of Al–Mn–Fe particles. Therefore, SSFSP should be regarded not only as a grain-refinement method, but also as a technique for corrosion localization control. Concerning the AZ31B magnesium alloy exposed to chlorides, the key advantage of the SSFSP technique lies in its ability to hinder localized penetration paths.

References

[1] Makar, G. L., & Kruger, J. L. (1993). Corrosion of magnesium. International materials reviews, 38(3), 138-153.

[2] Song, G. L., & Atrens, A. (1999). Corrosion mechanisms of magnesium alloys. Advanced engineering materials, 1(1), 11-33.

[3] Gray, J., & Luan, B. (2002). Protective coatings on magnesium and its alloys—a critical review. Journal of alloys and compounds, 336(1-2), 88-113.

[4] Frankel, G. S. (1998). Pitting corrosion of metals: a review of the critical factors. Journal of the Electrochemical society, 145(6), 2186-2198.

[5] Aung, N. N., & Zhou, W. (2010). Effect of grain size and twins on corrosion behaviour of AZ31B magnesium alloy. Corrosion Science, 52(2), 589-594.

[6] Bobby Kannan, M., Dietzel, W., & Zettler, R. (2011). In vitro degradation behaviour of a friction stir processed magnesium alloy. Journal of Materials Science: Materials in Medicine, 22(11), 2397-2401.
[7] Saikrishna, N., Reddy, G. P. K., Munirathinam, B., & Sunil, B. R. (2016). Influence of bimodal grain size distribution on the corrosion behavior of friction stir processed biodegradable AZ31 magnesium alloy. Journal of magnesium and alloys, 4(1), 68-76.
[8] Mishra, R. S., & Ma, D. Z. (2005). Friction stir welding and processing. Materials science and engineering: R: reports, 50(1-2), 1-78.
[9] Ma, Z. (2008). Friction stir processing technology: a review. Metallurgical and materials Transactions A, 39(3), 642-658.
[10] Patel, V., Li, W., Vairis, A., & Badheka, V. (2019). Recent development in friction stir processing as a solid-state grain refinement technique: microstructural evolution and property enhancement. Critical Reviews in Solid State and Materials Sciences, 44(5), 378-426.
[11] Argade, G. R., Kandasamy, K., Panigrahi, S. K., & Mishra, R. S. (2012). Corrosion behavior of a friction stir processed rare-earth added magnesium alloy. Corrosion Science, 58, 321-326.
[12] Nia, A. A., Omidvar, H., & Nourbakhsh, S. H. (2014). Effects of an overlapping multi-pass friction stir process and rapid cooling on the mechanical properties and microstructure of AZ31 magnesium alloy. Materials & Design, 58, 298-304.
[13] Darras, B., & Kishta, E. (2013). Submerged friction stir processing of AZ31 Magnesium alloy. Materials & Design, 47, 133-137.
[14] Liu, Q., Ma, Q. X., Chen, G. Q., Cao, X., Zhang, S., Pan, J. L., ... & Shi, Q. Y. (2018). Enhanced corrosion resistance of AZ91 magnesium alloy through refinement and homogenization of surface microstructure by friction stir processing. Corrosion science, 138, 284-296.
[15] Huang, L., Wang, K., Wang, W., Yuan, J., Qiao, K., Yang, T., ... & Li, T. (2018). Effects of grain size and texture on stress corrosion cracking of friction stir processed AZ80 magnesium alloy. Engineering Failure Analysis, 92, 392-404.
[16] Chai, F., Zhang, D., & Li, Y. (2015). Microstructures and tensile properties of submerged friction stir processed AZ91 magnesium alloy. Journal of Magnesium and Alloys, 3(3), 203-209.
[17] Cao, G., Zhang, D., Chai, F., Zhang, W., & Qiu, C. (2016). High-Strain-Rate Superplasticity in Mg–Y–Nd Alloy Prepared by Submerged Friction Stir Processing. Advanced Engineering Materials, 18(2), 312-318.
[18] Patel, V., Li, W., & Xu, Y. (2019). Stationary shoulder tool in friction stir processing: a novel low heat input tooling system for magnesium alloy. Materials and manufacturing processes, 34(2), 177-182.
[19] Patel, V., Li, W., Liu, X., Wen, Q., Su, Y., Shen, J., & Fu, B. (2020). Tailoring grain refinement through thickness in magnesium alloy via stationary shoulder friction stir processing and copper backing plate. Materials Science and Engineering: A, 784, 139322.
[20] Sejani, D., Li, W., & Patel, V. (2022). Stationary shoulder friction stir welding–low heat input joining technique: a review in comparison with conventional FSW and bobbin tool FSW. Critical Reviews in Solid State and Materials Sciences, 47(6), 865-914.
[21] Patel, V., Li, W., Andersson, J., & Li, N. (2022). Enhancing grain refinement and corrosion behavior in AZ31B magnesium alloy via stationary shoulder friction stir processing. journal of materials research and technology, 17, 3150-3156.
[22] Song, G., Atrens, A., Wu, X., & Zhang, B. (1998). Corrosion behaviour of AZ21, AZ501 and AZ91 in sodium chloride. Corrosion science, 40(10), 1769-1791.
[23] Esmaily, M., Svensson, J. E., Fajardo, S., Birbilis, N., Frankel, G. S., Virtanen, S., ... & Johansson, L. G. (2017). Fundamentals and advances in magnesium alloy corrosion. Progress in Materials Science, 89, 92-193.
[24] Gusieva, K. D. C. H. J., Davies, C. H. J., Scully, J. R., & Birbilis, N. (2015). Corrosion of magnesium alloys: the role of alloying. International Materials Reviews, 60(3), 169-194.
[25] Mandelbrot, B. B. (1983). The fractal geometry of nature/Revised and enlarged edition. New York.
[26] Costa, J. M., Sagues, F., & Vilarrasa, M. (1991). Fractal patterns from corrosion pitting. Corrosion science, 32(5-6), 665-668.
[27] Sarkar, N., & Chaudhuri, B. B. (1994). An efficient differential box-counting approach to compute fractal dimension of image. IEEE Transactions on systems, man, and cybernetics, 24(1), 115-120.
[28] Xu, S., & Weng, Y. (2006). A new approach to estimate fractal dimensions of corrosion images. Pattern Recognition Letters, 27(16), 1942-1947.
[29] Soille, P., & Rivest, J. F. (1996). On the validity of fractal dimension measurements in image analysis. Journal of visual communication and image representation, 7(3), 217-229.
[30] Nayak, S. R., Mishra, J., & Palai, G. (2019). Analysing roughness of surface through fractal dimension: A review. Image and Vision Computing, 89, 21-34.